BIOCHEMISTRY
including biophysical chemistry & molecular biology

Article

pubs.acs.org/biochemistry

Primary Photochemistry of the Dark- and Light-Adapted States of the YtvA Protein from *Bacillus subtilis*

Sang-Hun Song,[†] Dorte Madsen,[†] Jeroen B. van der Steen,[‡] Robert Pullman,[†] Lucy H. Freer,[†] Klaas J. Hellingwerf,[‡] and Delmar S. Larsen*[,†]

[†]Department of Chemistry, University of California at Davis, One Shields Avenue, Davis, California 95616, United States

[‡]Molecular Microbial Physiology Group, Swammerdam Institute for Life Sciences (SILS), University of Amsterdam, 1090 GE Amsterdam, The Netherlands

Supporting Information

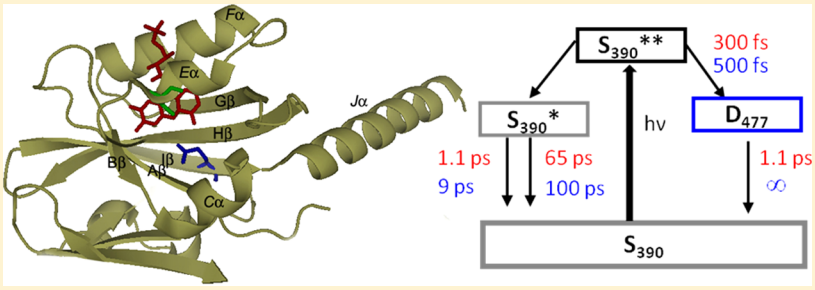

ABSTRACT: The primary (100 fs to 10 ns) and secondary (10 ns to 100 μs) photodynamics in the type II light−oxygen−voltage (LOV) domain from the blue light YtvA photoreceptor extracted from *Bacillus subtilis* were explored with transient absorption spectroscopy. The photodynamics of full-length YtvA were characterized after femtosecond 400 nm excitation of both the dark-adapted D_{447} state and the light-adapted S_{390} state. The S_{390} state relaxes on a 43 min time scale at room temperature back into D_{447}, which is weakly accelerated by the introduction of imidazole. This is ascribed to an obstructed cavity in YtvA that hinders access to the embedded FMN chromophore and is more open in type I LOV domains. The primary photochemistry of dark-adapted YtvA is qualitatively similar to that of the type I LOV domains, including AsLOV2 from *Avena sativa*, but exhibits an appreciably higher (60% greater) terminal triplet yield, estimated near the maximal Φ_{ISC} value of ≈78%; the other 22% decays via non-triplet-generating fluorescence. The subsequent secondary dynamics are inhomogeneous, with three triplet populations co-evolving: the faster-decaying ^{I}T* population (38% occupancy) with a 200 ns decay time is nonproductive in generating the S_{390} adduct state, a slower ^{II}T* population (57% occupancy) exhibits a high yield (Φ_{adduct} ≈ 100%) in generating S_{390} and a third (5%) ^{III}T*population persists (>100 μs) with unresolved photoactivity. The ultrafast photoswitching dynamics of the S_{390} state appreciably differ from those previously resolved for the type I AcLOV2 domain from *Adiantum capillus-veneris* [Kennis, J. T., et al. (2004) *J. Am. Chem. Soc. 126*, 4512], with a low-yield dissociation (Φ_{dis} ≈ 2.5%) reaction, which is due to an ultrafast recombination reaction, following photodissociation, and is absent in AcLOV2, which results in the increased photoswitching activity of the latter domain.

Homeostatic responses of organisms to external stimuli are both pervasive and crucial for sustaining life across all kingdoms on Earth. These important responses rely on complex multistep signaling pathways [e.g., signal transduction (receptors) → signal transmission → biological activity (effectors)] to operate. While these pathways can be initiated by chemical, temperature, or stress-based triggers, one such class of responses, particularly of interest to biophysicists, is light-induced and provides the possibility for coupling light into new biological responses via emerging optogenetic techniques.[1,2] The initial signal transduction steps of such pathways involve the photoexcitation of specialized chromophore-containing proteins that act as photoreceptors and are responsible for many biologically relevant functions, including vision, phototaxis, gene expression, and phototropism.[3,4]

YtvA from the soil bacterium *Bacillus subtilis* is an example of such a photoreceptor protein.[5] *B. subtilis* has a general stress response that is activated by a wide range of stresses, which can be subdivided into energy stresses (e.g., starvation of glucose) and environmental stresses (e.g., salt shock and alcohol shock).[6] The activity of the general stress response is regulated by a complicated signal transduction network that ultimately results in the release of the alternative sigma factor σ^{B},[6] which controls the GSR regulon of approximately 200 genes.[6−10]

YtvA is responsible for the activation of the environmental stress pathway in response to blue light.[11,12] The most upstream component of this pathway is a large protein complex

Received: September 4, 2013
Revised: October 10, 2013
Published: October 11, 2013

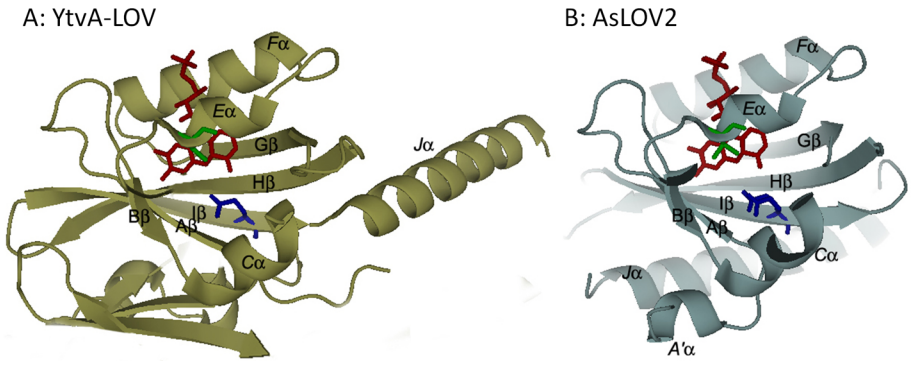

Figure 1. X-ray crystal structures of the slowly recovering YtvA-LOV domain (PDB entry 2PR6) and the LOV2 domain from phototropin of AsLOV2 (PDB entry 2V1B). The primary difference is that the J α-helix, which contacts the primary β-sheet on the opposite side of the FMN chromophore (red molecule) in AsLOV2, is splayed out to connect the STAS domain (not shown) to the LOV domain in YtvA. The cyteine (in two conformations) is colored blue.

called the "stressosome", which consists of two to (at least) six different proteins *in vivo*.[13,14] YtvA and all known components of the stressosome have a C-terminal STAS (sulfate transporter and anti-σ factor antagonist) domain,[15] suggesting that YtvA may also be part of the stressosome. Indeed, YtvA is copurified with stressosome components[12] and can be incorporated into stressosomes *in vitro*,[16] and its function is dependent on the composition of the stressosome *in vivo*.[17] Light activation of YtvA results in the release of the kinase RsbT from the stressosome, which ultimately results in the release of σ^B through several intermediate steps.[6]

The YtvA protein comprises two domains: a light−oxygen−voltage (LOV) sensitive domain (ranging from amino acid 25 to 126) that is linked to a STAS domain (from amino acid 148 to 261).[18] LOV domains are a structural prototype for the broadly distributed Per-Arnt-Sim (PAS, for period circadian protein, Ah receptor nuclear translocator protein, and single-minded protein) class of signal transduction proteins that are responsible for the activation of many pathways (both light-initiated and non-light-initiated).[19] PAS domains are found primarily in proteins that are involved directly or indirectly in signal transduction,[20] which includes a wide spectrum of proteins involved in cell responses to changes in environmental and intracellular conditions such as histidine and serine/threonine kinases, chemoreceptors, circadian clock proteins, voltage-activated ion channels, cyclic nucleotide phosphodiesterases, regulators of responses to hypoxia,[21] proteins involved in the embryological development of the central nervous system,[22] and photoreceptors for taxis and tropism.[23] LOV domains often bind noncovalently to a flavin molecule, and YtvA specifically binds the mononucleotide (FMN) chromophore that initiates its light response upon photoexcitation.[15,24]

As with the larger PAS family, LOV domains are ubiquitous in nature and are found in many light-activated photosensitive proteins. The plant phototropic sensory protein phototropin 1 consists of two LOV domains (LOV1 and LOV2) coupled to a Ser-Thr kinase activity domain in the C-terminal region.[24] The structure and photodynamics of the phototropin 1 LOV2 domain from *Avena sativa* (AsLOV2) and the LOV2 domain extracted from the phy3 receptor of *Adiantum capillus-veneris* (AcLOV2)[25] have been extensively studied via multiple techniques, including ultrafast (femtoseconds to nanoseconds) transient spectroscopy.[26−28] LOV domains are of particular interest for both basic science and engineering applications, many of which are based on emerging optogenetic approaches to conferring photosensitivity to target proteins via genetic fusion of LOV domains to exogenous targets.[1,2]

The general mechanism of LOV photodynamics involves blue light illumination of the dark-adapted state (D_{447}) to generate a singlet excited state D_{447}* that then evolves rapidly into a reactive triplet state T* with a high yield.[28,29] This, in turn, generates a FMN−cysteine photoadduct,[29,30] and the subsequent changes in the hydrogen bonding network alter the protein structure (often involving large scale rearrangements)[29,30] to generate the light-adapted state (S_{390}).[23] LOV domains can be separated into two categories based on the rate of the thermally activated dark recovery ($S_{390} \rightarrow D_{447}$) reaction: type I domains, which are found in plant phototropins, and type II domains, which are found in bacteria and fungi. The LOV domain in YtvA from *B. subtilis* is a type II domain.[31,32] While type I domains exhibit several second recovery kinetics, type II LOV domains exhibit slow thermal recovery kinetics (i.e., 30−60 min at room temperature).[28] Despite the differing recovery kinetics, both type I and type II LOV domains are structurally similar (Figure 1).[33] The LOV domain of YtvA is similar to AcLOV2 from *A. capillus-veneris* with a few key differences. A salt bridge between the D α-helix (Dα) and the G β-sheet (Gβ) in AcLOV2 is destabilized in the light-induced state (not shown),[34] while a salt bridge in the YtvA-LOV domain stabilizes the light-induced structural change.[33] Moreover, the YtvA-LOV domain was determined to be dimeric *in vitro*.[35−37] L106, I108, and F119, residues located at the interface of the two monomers, minimize the structural change of YtvA in the light-adapted S_{390} state,[33] which inhibits significant conformational rearrangements after photoexcitation, like the partial unfolding of the (equivalent of the) J α-helix, which forms the signaling state in AsLOV2.[38,39] In YtvA, this helix is splayed out from the LOV domain, and the STAS domain is bound to this protruding helix (Figure 1).[38,39]

The fluctuation dynamics of the protein, especially of the residues near the flavin, strongly influence its primary photodynamics. For example, thermal isomerization of Cys434 in AsLOV2 modulates the intersystem triplet formation rates by oscillating the proximity of the heavy atom sulfur atom to the flavin chromophore.[40−42] Hence, the different LOV structures and corresponding protein dynamics may strongly modulate both their photodynamics and the resulting photoactivity, and it is not unexpected that the primary photodynamics of YtvA are different from those of the type I LOV domains that have been previously characterized.

dx.doi.org/10.1021/bi4012258 | *Biochemistry* 2013, 52, 7951−7963

The S_{390} adduct population in LOV domains exhibits photoactive properties as first demonstrated by Kennis et al.,[26] who resolved the dynamics underlying the ultrafast photoswitching activity between the S_{390} and D_{447} states of the type I AcLOV2 domain. The reverse reaction ($S_{390} \rightarrow D_{447}$) results from an excited-state photodissociation mechanism with the rapid breaking of the FMN−cysteinyl bond and hydrogen extraction of the C4a proton of the S_{390} adduct to generate an intermediate population with a spectrum that strongly resembles that of the dark-adapted D_{447} population (termed I_{447}), but with the surrounding protein still set within the S_{390} structure. The secondary dynamics of this adduct photodissociation reaction in YtvA were resolved by Losi and co-workers[43] and Hellingwerf and co-workers,[44] who both demonstrated that this photoswitching activity is considerably less efficient in YtvA than in other LOV domains. However, the origin of this low yield is unclear and may result from the initial photodissociation event or from the subsequent dynamics, which requires direct probing of the transient dynamics to be addressed.

No study to date has resolved the primary (<10 ns) photochemical dynamics of the D_{447} state in YtvA, which are responsible for initiating the type II photocycle. Moreover, the primary dynamics of the dissociation dynamics of S_{390} have not been characterized. Presented here is the first ultrafast transient absorption study of the photoinitiated dynamics of the dark-adapted and light-adapted adduct state of the YtvA protein in *B. subtilis*. Although Losi et al. characterized the secondary (>10 ns) photodynamics of the dark-adapted D_{447} state of YtvA,[5] the secondary dynamics of the dark-adapted population were also measured here to bridge the 12-decade gap (femtoseconds to milliseconds) between ultrafast exited-state dynamics and the dynamics of adduct formation.

MATERIALS AND METHODS

Sample Preparation. Full-length YtvA with an N-terminal six-His tag was isolated from production host *Escherichia coli* M15/pREP4 (QIAGEN) carrying the pQE-30-ytvA plasmid.[11] Cells were routinely grown at 37 °C while being shaken at 250 rpm in production broth (PB) (5 g/L glucose, 20 g/L Bacto-trypton, 10 g/L yeast extract, 5 g/L NaCl, and 8.7 g/L K_2HPO_4), supplemented with 50 μg/mL kanamycin and 100 μg/mL ampicillin to maintain the plasmids. A production culture was inoculated with cells from a fresh plate, which was allowed to grow until an optical density at 600 nm (OD_{600}) of ∼0.3 was reached. Cells were then diluted to an OD_{600} of ∼0.15 in 2 L of PB. After the cultures had reached an OD_{600} of ∼0.3, expression of YtvA was induced via the addition of IPTG to a final concentration of 0.2 mM. The cultures were then moved to a shaking incubator at room temperature and incubated overnight. Cells were harvested by centrifugation, and cell-free extract was prepared by sonication in buffer [20 mM Tris-HCl, 10% glycerol, and 10 mM NaCl (pH 8)].

The YtvA protein was isolated from the cell-free extract using an ÄKTA FPLC system (GE Healthcare) with a HisTrap HP 5 mL column (GE Healthcare) and eluted with a linear gradient from 20 to 500 mM imidazole in a buffer that consisted of 20 mM Tris-HCl and 100 mM NaCl (pH 8.0). YtvA-containing fractions were pooled and dialyzed against 20 mM Tris-HCl (pH 8.0). The protein was further purified on a Resource Q column (GE Healthcare) using a linear gradient from 0 to 0.4 M NaCl in a buffer with 20 mM Tris-HCl (pH 8.0). Fractions containing the protein (which eluted at ∼0.1 M NaCl) were pooled and concentrated on a Corning Spin-X UF Concentrator (10 kDa), and the buffer was exchanged with 20 mM Tris-HCl (pH 8.0) for storage. This protein isolation procedure is similar, but not identical, to the procedure described elsewhere,[44] and all TA signals were measured at room temperature. The samples used in the transient dynamics were full-length YtvA (i.e., LOV-STAS).

Isolated YtvA-LOV domains for the dark recovery dynamics were produced with a different protocol involving the expression of the Novagen pET15b vector (EMD Chemicals, Gibbstown, NJ) in *E. coli* BL21(DE3) and then purified from cell extracts. The expression vector was constructed by T. Gaidenko;[15] an 800 bp fragment containing the *ytvA* coding sequence was amplified from the *B. subtilis* genome using primers ytvNB1 (5′-AGGGGGATTCATATGGCTAGTTTT-CAATC-3′) and ytvNB2 (5′-GTGAGCGGGATCCTTTTAC-ATAATCGGAA-3′), containing *Nde*I and *Bam*HI sites, respectively (underlined). This fragment was cloned into the *Nde*I and *Bam*HI sites of pET15b to create pTG5502. Here we induced expression in a 500 mL culture of *E. coli* BL21(DE3) by adding IPTG; the protein was purified under native conditions by being passed over a nickel affinity column, according to the manufacturer's protocols (Qiagen Inc., Valencia, CA). This yielded 30 mg of protein in 2 mL of elution buffer [50 mM NaH_2PO_4, 300 mM NaCl, and 250 mM imidazole (pH 8.0)], determined by the Protein Assay Reagent (Bio-Rad Laboratories, Hercules, CA). The protein was judged to be >95% pure by sodium dodecyl sulfate−polyacrylamide gel electrophoresis and Coomassie staining (not shown).

Experimental Setups. Ultrafast (<10 ns) transient absorption spectra were measured with a Ti:sapphire laser system (Spectra Physics Spitfire Pro and Tsunami) outlined in detail elsewhere.[45] The 800 nm pulsed laser output was delivered with an energy of 2.25 mJ at a repetition rate of 1 kHz and a 40 fs (full width at half-maximum) duration. The laser beam was split into two equal-length pathways: one for the pump and another for the probe. The 400 nm pulses used for exciting both dark- and light-adapted populations were generated by frequency doubling of the 800 nm pulses in a β-barium borate crystal (0.5 mm thick, 29.2°). The intensity of the pump pulse used to excite the YtvA domain was 1.3 μJ for both dark- and light-adapted states. White light probe pulses were generated by focusing 800 nm light on a CaF_2 crystal. The polarization of the pump and probe beams were set to the magic angle (54.7°) with respect to each other. The sample was recirculated at room temperature through a 2 mm × 2 mm quartz flow cell to avoid photodegradation and refreshed between laser shots with a peristaltic pump (Watson-Marlow Sci-Q 400 series). Because of the long recovery time of S_{390} in YtvA,[31] and the extensive spectral overlap of the absorption spectra of the D_{447} and S_{390} states (see below), the signals from the dark-adapted state may contaminate the desired light-induced signals. To avoid this, the full-length YtvA sample was circulating through a flow cell every 60 s and was continuously exposed to a 473 nm laser diode (2.5×10^{-2} W/cm^2) during data collection. This shifted the sample nearly exclusively into the S_{390} population, which was confirmed via monitoring the ground-state absorption spectrum during the experiment. Moreover, no contaminating D_{447}-induced signals were observed in the measured light-adapted S_{390} signals, or vice versa. The instrument response function (IRF) time scale is estimated to be 120 fs for the ultrafast signals of both types of primary measurements described below.

dx.doi.org/10.1021/bi4012258 | *Biochemistry* 2013, 52, 7951−7963

The instrumental setup for measuring the secondary dynamics was based on a design similar to that of the ultrafast apparatus described above with two primary differences. (1) The broadband probe pulses generated by focusing a portion (~1 μJ) of the 800 nm amplified pulses into a slowly translating 10 mm thick CaF_2 crystal were imaged via a spectrograph (Oriel Instruments) onto a 512-pixel silicon diode array. (2) The excitation pulses used for initiating the secondary signals were generated in a separate, independently Q-switched diode-pumped solid-state Nd:YAG (neodymium-doped yttrium aluminum garnet) laser (Alphalas-A-532-300), in contrast to the 400 nm pulses used in the ultrafast apparatus. The resulting 355 nm pulses were generated by the third harmonic generation of the YAG's 1064 nm fundamental light via a 5 mm thick potassium dihydrogen phosphate crystal. Its IRF time was estimated to be ~500 ps, using the signal rise times of the data as a reference.

Static UV–vis absorbance spectra of YtvA samples (in the D_{447} and S_{390} states) were recorded with an unmodified Shimadzu UV–vis (UV-1700) spectrophotometer. Dark recovery kinetics were measured with the same spectrometer after exposing the dark-adapted D_{447} sample to a 473 nm laser diode (300 mW) for 10 s to generate the S_{390} population and then collecting full absorption spectra of the sample every 2 min up to 120 min as the D_{447} population was thermally repopulated.

Global Analysis. All transient data sets were analyzed with global analysis techniques that fit the data to multipopulation models of co-evolving time-dependent populations with time-independent spectra.[46,47] This approach involves solving a system of linear differential equations that describe a specific "target model" to generate the best fit to the data, subject to photophysical constraints. Prior to the construction of the target model, each data set was independently analyzed within a sequential model (see Supporting Information) to generate unbiased evolution-associated difference spectra (EADS), which are the averaged spectral signatures of "compartments" with increasing lifetimes. While the EADS often do not represent the spectra of a single constituent species in the measured dynamics (especially for ultrafast data), nevertheless, valuable information can be extracted from such an analysis through simple manipulations to aid subsequently in constructing viable target models.[48,49] In particular, this approach is useful in estimating the relevant number of distinct compartments (i.e., populations) in the target model and the associated apparent (i.e., directly observed from the data) time constants. Decomposing the apparent kinetics into underlying microscopic kinetics (i.e., evolution from the population of one state to another) requires further modeling with a target analysis.[46,47]

A "target analysis" estimates the time-independent species-associated difference spectra (SADS) with corresponding time-dependent concentration profiles of the populations within a target model.[46,47] This is accomplished by fitting the data with numerical solutions of first-order linear differential equations describing a postulated model (eq 1):

$$\frac{dn_1}{dt} = A_i I(t) + \sum_j K_{ij} n_j \quad (1)$$

with n_i representing the i^{th} microscopic population of interest, $A_i I(t)$ the pump pulse temporal width, and K the rate constant matrix that describes the exponential behavior of transitions from one population into another. The integrated solutions to the linear differential equations in eq 1 simulate transient populations evolving with single-exponential microscopic kinetics.[46–49]

RESULTS

The static absorption spectrum of the dark-adapted D_{447} state of YtvA (Figure 2A, red structure) exhibits a strong vibronic

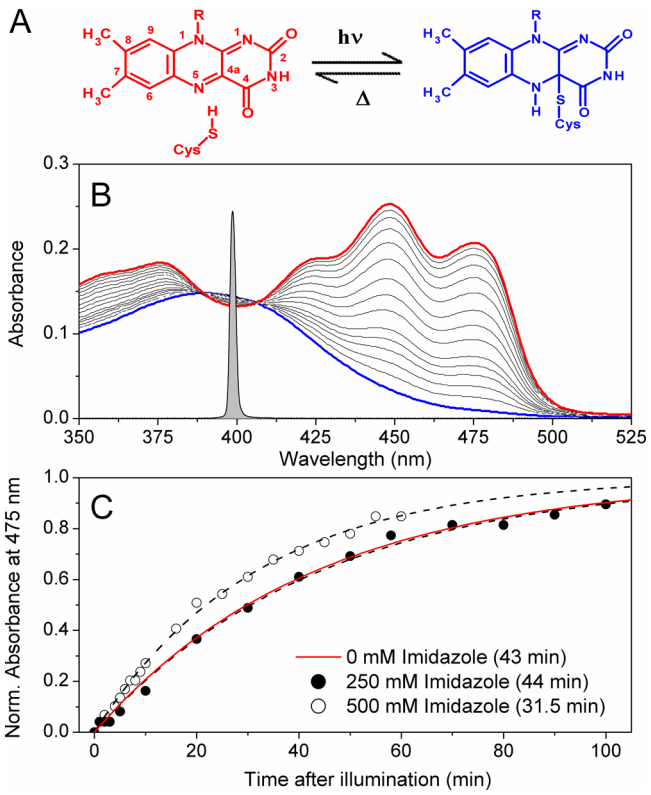

Figure 2. (A) Schematic representation of the photochemical formation of the cysteine–FMN photoadduct in the LOV domain from YtvA. (B) Absorption spectra for the dark recovery of the YtvA-LOV domain (no STAS) from *B. subtilis* in 50 mM NaH_2PO_4, 300 mM NaCl, and 500 mM imidazole (pH 8). The dark-adapted D_{447} sample was exposed with a 473 nm laser diode for 10 s to generate the S_{390} population. The solid gray-filled curves represent the spectra of the excitation pulses used in the primary (400 nm) and secondary (355 nm) measurements. The arrow shows the recovery kinetics from S_{390} to D_{447}. (C) The time constant of the thermal recovery kinetics is 44 min at 250 mM imidazole and 31.5 min at 500 mM imidazole. The solid red curve is the recovery process in the absence of imidazole.[31]

structure with peaks at 422, 447, and 474 nm that are ascribed to the lowest-energy $S_0 \rightarrow S_1$ electronic transition (Figure 2B, red curve) of the FMN chromophore. A second, higher-energy $S_0 \rightarrow S_2$ electronic transition overlaps the $S_0 \rightarrow S_1$ transition and peaks near 365 nm.[50] Irradiation of the YtvA-LOV domain in the dark-adapted D_{447} population generates the metastable S_{390} photoadduct population (Figure 2A, blue structure) with a smooth Gaussian-like spectrum peaking at 390 nm (Figure 2B, blue curve). This S_{390} population then slowly decays (τ = 43 min at room temperature) to re-form the dark-adapted D_{447} state as the FMN–Cys bond is hydrolyzed.

Adding imidazole to type I, fast-cycling LOV domains significantly accelerates the thermally activated $S_{390} \rightarrow D_{447}$ recovery kinetics.[32,51] For example, the recovery time scales of

dx.doi.org/10.1021/bi4012258 | *Biochemistry* 2013, 52, 7951–7963

AsLOV2 are accelerated 2800-fold after the introduction of 500 mM imidazole.[52] However, the slower 43 min recovery kinetics for the type II LOV domain of YtvA (Figure 2C, red curve) are only slightly accelerated (i.e., 36% to 31.5 min) after the addition of 500 mM imidazole [Figure 2C (○)]. A key step in the recovery kinetics is the transfer of a proton from the N5 position of the FMN adduct (Figure 2A, blue structure) to the reactive Cys, which leads to hydrolysis of the FMN−Cys bond.[52] Imidazole purportedly facilitates this step by directly abstracting the proton,[51] which requires relatively unhindered access of imidazole to the FMN chromophore binding pocket for reasonable efficiency.

Two cavities have been suggested for providing imidazole access to the N5 region of the FMN chromophore:[52] (1) the Aβ−Bβ strands and (2) the area enclosed by Cα and Hβ.[51] The FMN binding pocket is strongly conserved over both type I and type II LOV domains,[33] which facilitates the comparison of YtvA (PDB entry 2PR6) with other LOV domains with known crystal structures, including AsLOV2 (PDB entry 2V1B), AcLOV2 (PDB entry 1JNU), and the LOV1 domain from *Chlamydomonas reinhardtii* (CrLOV1) (PDB entry 1N9O). Comparison of the two cavities for the four LOV domains (Figure S1 of the Supporting Information) shows that the Aβ−Bβ cavity does not differ significantly in size or geometry (Table 1). However, the Cα−Hβ cavity is distinctly smaller

Table 1. Relative Cross Sections for Proposed Cavities for Solvent-Exposed Imidazole Access to the FMN Chromophore[a]

relative cross section	YtvA-LOV	AcLOV2	AsLOV2	CrLOV2
Aβ−Bβ strand cavity	1	0.903	0.988	0.937
Cα−Hβ cavity	1	1.47	1.48	1.56

[a]The reduced size of the Cα−Hβ in YtvA was primarily due to the rotation of Phe46 by 150° with respect to other LOV domains (Figure 3 and Figures S1 and S2 of the Supporting Information).

(30%) in YtvA-LOV than in the other three LOV domains (Figure S2 of the Supporting Information), which is primarily a consequence of the rotation of Phe46 by 150° with respect to other LOV domains (Figure 3, red residues). Presumably, this

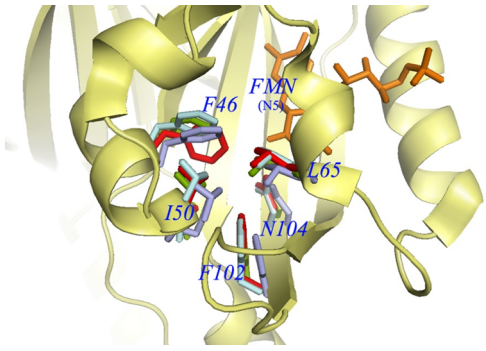

Figure 3. Cα−Hβ cavity resolved from the crystal structures for *B. subtilis* YtvA-LOV (PDB entry 2PR6) (red) overlaid with other LOV domains, including AcLOV2 (PDB entry 1JNU, green), AsLOV2 (PDB entry 2V1B, cyan), and CrLOV2 (PDB entry 1N9O, violet). The aromatic ring of Phe46 in YtvA in YtvA is rotated with respect to other LOV domains and extends into the cavity, presumably to hinder the access of imidazole to the FMN (orange) (see Figure S2 of the Supporting Information for more details). The backbones of the four structures were aligned via PyMol.

smaller cavity hinders access of imidazole to the N5 region of FMN and reduces its effectiveness in accelerating the recovery kinetics of YtvA. Despite the inability to externally facilitate faster recovery kinetics in wild-type YtvA by adding imidazole, the transient signals presented below were measured without resolvable complications from the long-living nature of YtvA-S_{390} (as confirmed by the lack of contamination in the TA signals). This is due to a combination of fast recirculation times, large sample reservoirs, and weak excitation pulses.

Primary D_{447} Photodynamics (100 fs to 10 ns). The ultrafast TA spectra measured after photoexcitation of the D_{447} state of YtvA extend across the entire visible spectrum (Figure 4). Although 400 nm excitation introduces excess vibrational

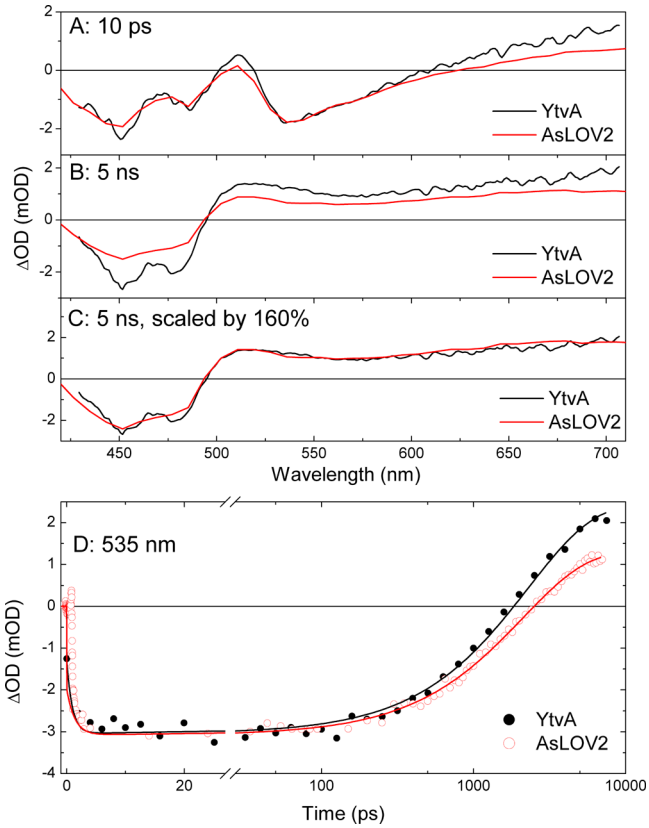

Figure 4. Comparison of the ultrafast (<8 ns) photodynamics of the forward reaction dynamics of full-length YtvA (black curves) with the dynamics of the AsLOV domain (red curves)[28] after 400 nm excitation. (A) The 10 ps transient spectra of the singlet excited state of the FMN in D_{447}. (B) The 5 ns spectrum of the T* spectrum 5 ps after scaling the two data sets to time spectra with similar amplitudes. (C) The 5 ns spectrum for AsLOV2 is scaled by 160% and compared to the 5 ns spectrum for YtvA. (D) The intersystem kinetics at 535 nm showing the 60% higher triplet yield of full-length YtvA (●) vs that of AsLOV2 (red ○). The solid curves are the respective fits to the target model in Figure 7A.

energy (~3500 cm^{-1}) into the system, as compared to the use of a lower-energy wavelength (at 470 nm), it has previously been established that excitation wavelengths between 360 and 470 nm induce similar photocycles and quantum yields;[53,54] this excitation wavelength independence (neglecting vibrational relaxation) also extends to the primary and secondary dynamics (Figure S3 of the Supporting Information) as discussed below. Photoexcitation of D_{447} generates the singlet excited-state D_{447}* population with a characteristic spectrum consisting of a

dx.doi.org/10.1021/bi4012258 | *Biochemistry* 2013, 52, 7951−7963

ground-state bleach (GSB) between 400 and 500 nm, a (negative) stimulated emission (SE) band near 540 nm, and an overlapping broad and structured positive excited-state absorption (ESA), ranging from 510 to >700 nm (Figure 4A, 10 ps spectrum). This latter spectrum is similar to the singlet excited-state spectrum identified for oxidized FMN[55] and is nearly identical to previously reported D_{447}* signals reported for other LOV domains.[27,28,51] On a ~2 ns time scale, the excited-state D_{447}* population evolves into a new population with a broad ESA extending from 490 nm to the red and overlapping a (negative) GSB from <490 nm (Figure 4B, 5 ns spectrum). This spectrum is identical to the previously resolved triplet-state (T*) spectrum of flavins[56] and is observed in the primary dynamics of other LOV domains.[27,28,51] In addition, a rapid subpicosecond evolution preceding the generation of T* is resolved as a blue-shifting SE. This is ascribed to vibrational cooling of the D_{447}* population (Figure S3B of the Supporting Information, dashed black curve)[55] because it is not observed in TA signals initiated with lower-energy (e.g., 470 nm) excitation of FMN;[27,51] its presence does not alter the subsequent dynamics.

The (D_{447}* → T*) singlet to triplet intersystem crossing (ISC) kinetics in YtvA (Figure 4) strongly resemble the reported dynamics of other LOV domains,[27,28,51] including the fast-cycling AsLOV2[28] and AcLOV2 domains,[27] with similar time scales. In fact, the ISC time scales for YtvA and AsLOV2 are nearly identical (Figure 4D) but do exhibit distinctly different triplet yields. Assuming identical extinction coefficients for the respective D_{447}* and T* populations in both YtvA and AsLOV2, YtvA has a 60% higher ISC quantum yield (Φ_{ISC}) as indicated by the scaled terminal spectra in Figure 4C. Using the reported value of 65% for Φ_{ISC} of AsLOV2[27] suggests that YtvA has a near-unity triplet yield ($\Phi_{ISC} \approx 100\%$). However, Losi et al.[5] estimated that 22% of the excited-state D_{447}* population of YtvA is quenched via radiative emission, which provides an upper limit of 78% for the ISC yield and suggests that the estimate of Φ_{ISC} of 65% for AsLOV is overestimated.

Secondary D_{447} Photodynamics (10 ns to 100 μs). The 355 nm initiated secondary dynamics after excitation of D_{447} track the evolution of T* into the S_{390} adduct population from 10 ns to 100 μs (Figure 5). As expected, the D_{447}* ISC signals are weakly dependent on excitation wavelength with similar dynamics (other than time resolution and amplitude) after either 400 or 355 nm excitation (Figure S4 of the Supporting Information). The resulting T* population (ascribed on the basis of the similarity to previously resolved triplet-state spectra of flavins[56] and other LOV domains[27,28,51]) persists into the microsecond time scale and decays with biphasic kinetics (Figure 5B), with an additional nondecaying (>100 μs) population that is tentatively ascribed to a long-living triplet population (with a spectrum very comparable to that of the faster T* populations) similar to those observed in cysteine-less mutants of CrLOV2 (Table S1 of the Supporting Information).[57] No nonlinear excitation power features of the signals were observed (Figure S5 of the Supporting Information), which would have indicated that they would result from a multiphoton ionization pathway that contaminated the single-photon-initiated signals.[58] These nonexponential signals strongly suggest underlying inhomogeneous dynamics involving multiple coexisting T* populations evolving with nearly identical spectra, but with different kinetics (see modeling below). For the visible probe window (425−710 nm) of the data presented here, the bleach of D_{447} is used to resolve the formation of the terminal (on this time scale) S_{390} adduct population (Figure 5A, magenta curve), which is associated with the loss of the more red absorbing D_{447} (Figure 2B).

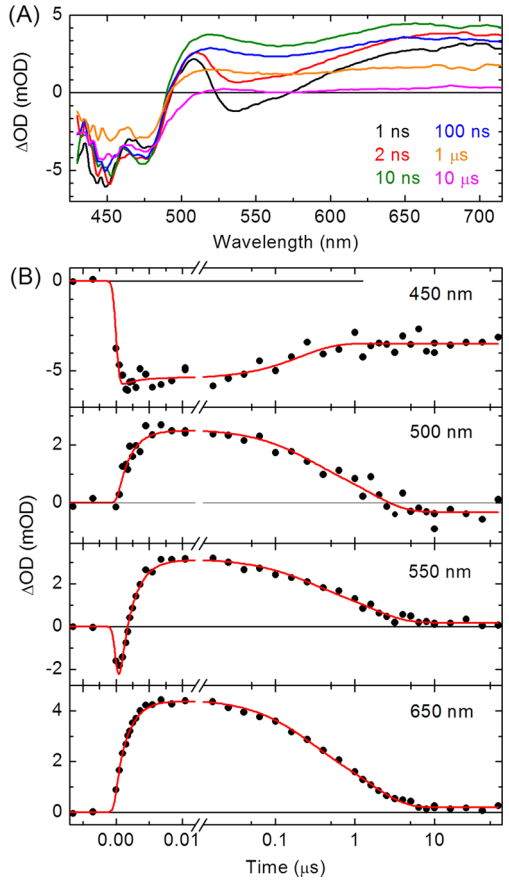

Figure 5. Dark-adapted D_{447} photodynamics of full-length YtvA initiated with 355 nm excitation. (A) Transient spectra at select probe times, as indicated, and (B) kinetics at select probe wavelengths, as indicated. The primary (<8 ns) photodynamics collected with ultrafast 400 nm pulses are nearly identical to those initiated with 355 nm excitation (Figures S3 and S4 of the Supporting Information). Raw data (●) are displayed with an overlapping four-compartment sequential fit (—) in Figure 8A. The primary kinetics are similar to the ultrafast kinetics measured for AsLOV2[28] as demonstrated in Figure 4.

Primary S_{390} Photodynamics (100 fs to 10 ns). The 400 nm initiated transient signals of the S_{390} adduct state (Figure 6) are appreciably different from the dark-adapted D_{447} initiated signals in Figures 4 and 5. The S_{390}-derived TA signals evolve nonexponentially, involving both decay and spectral evolution from the initial spectrum, which peaks at 600 nm (black curve), into broad ~510 nm absorbing spectra (green and blue curves) that eventually generate a weak terminal band that resembles the D_{447} population (magenta and dark red curves), with an even weaker far-red (>650 nm) absorption. The S_{390} bleach was observed only below 450 nm within the first picosecond, and no clearly resolved SE band was observed. These ultrafast signals from the light-adapted state in YtvA strongly resemble the TA signals measured after excitation of S_{390} in AcLOV2 by Kennis and co-workers (Figure S6 of the Supporting Information),[26] except that the YtvA signals decay ~2-fold faster.

dx.doi.org/10.1021/bi4012258 | Biochemistry 2013, 52, 7951−7963

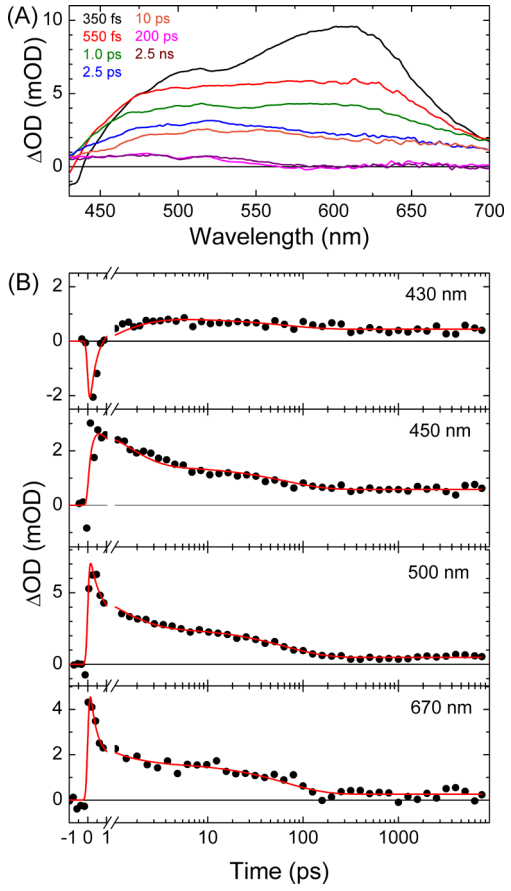

Figure 6. Ultrafast (<8 ns) signals after photoexcitation of the S_{390} adduct in full-length YtvA after 400 nm excitation. (A) Transient spectra at select probe times as indicated in the legend. (B) Kinetics (●) at select wavelengths with overlapping four-compartment sequential global analysis fits (—) from the sequential model in Figure 8A.

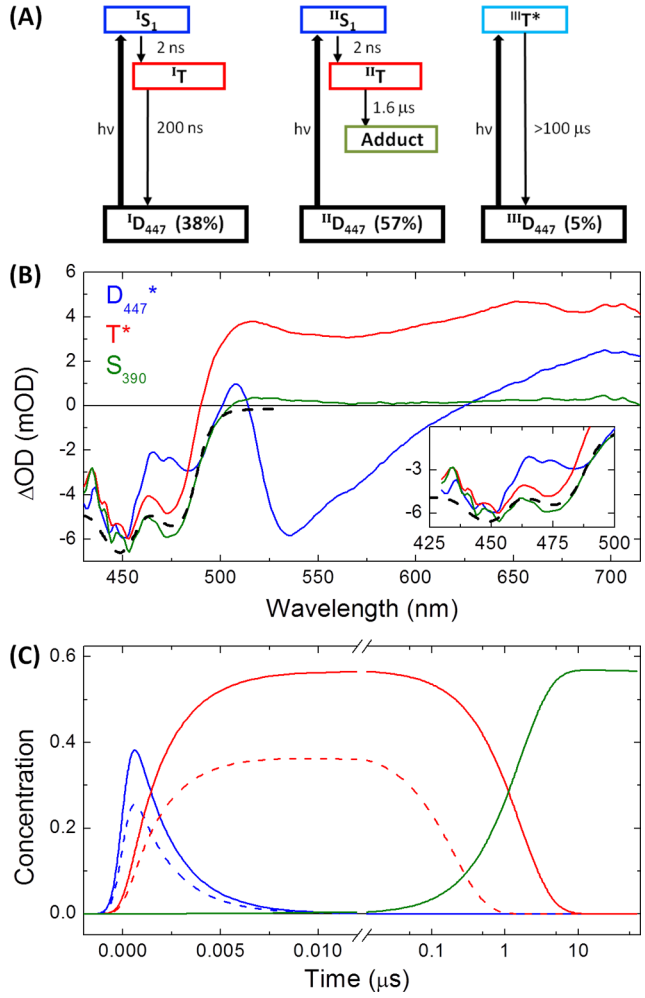

Figure 7. Target analysis of the secondary (<100 μs) TA signals of the dark-adapted D_{447} state in full-length YtvA after 355 nm excitation. (A) Proposed target model with (B) estimated SADS and (C) corresponding population profiles. The model has two coexisting excited-state D_{447}* populations (blue curves) evolving into three triplet subpopulations (red curves) on this time scale: ^{I}T* (red dashed curve), ^{II}T* (red solid curve), and ^{III}T* (shown in Figure S7 of the Supporting Information). The ^{I}T* population is inactive (38%) and decays directly into the bleach, while ^{II}T* (57%) generates S_{390}, modeled with a 100% yield here to simulate a comparable amplitude of the D_{447} bleach from 425 to 500 nm. The ^{III}T* population (cyan) is weakly observed, does not decay on the time scale of the experiment, and was not included in the primary dynamics only for the sake of convenience (Figure S7B of the Supporting Information for SADS). The fits of this model to the data can be observed in Figures 4 and 5.

DISCUSSION

Dark-Adapted D_{447} Photodynamics. The ultrafast signals of D_{447} in YtvA are dominated by the high-yield ISC dynamics that generate the reactive triplet (T*) populations (Figures 4 and 5). The primary dynamics for YtvA (and most other LOV domains) can be modeled with a single 2.1 ns exponential evolution (Figure 4D), with an assumption of homogeneous photodynamics with a single D_{447}* population and a single T* population. However, we previously reported a dynamic inhomogeneous model[28] to describe the ISC dynamics of the wild type and the F434Y mutant of AsLOV2, involving an interplay of conformational dynamics of the nearby cysteine (i.e., inhomogeneity) with ISC dynamics that are sensitive to the proximity of the sulfur atom in the cysteine to the flavin.[28] This '*dynamic* conformer model' reconciles the single-exponential ISC kinetics in wild-type AsLOV2 with the nonexponential ISC kinetics in the F434Y mutant of AsLOV2 and is further supported by molecular dynamics simulations.[28] While this model can also be applied for modeling the YtvA signals with its single-exponential ISC kinetics, a homogeneous model is sufficient (and considerably easier) to describe the data.

However, despite the ease of applying the homogeneous model and the presumed accuracy of the dynamic inhomogeneous model, the YtvA ultrafast signals here were modeled with a third and isomorphic *static* inhomogeneous model (Figure 7A) consisting of two D_{447}* populations with identical 2.1 ns ISC kinetics following a fast 1 ps vibrational cooling phase (Figure 7A and Figure S4 of the Supporting Information). The rationale for using this model for interpreting the YtvA signals (with results identical to those from the homogeneous model) is that the secondary signals are inhomogeneous (more below), which posits the existence of inhomogeneity in the primary dynamics, even if they are not directly observed (i.e., the inhomogeneity does not modulate the ISC kinetics). No effort was made to decompose the observed 2.1 ns kinetics into the underlying ISC and nonproductive decay channels (i.e., internal conversion and radiative decay).[27] However, clearly YtvA is better able to direct the excited-state evolution of D_{447}* into

dx.doi.org/10.1021/bi4012258 | *Biochemistry* 2013, 52, 7951−7963

higher-T* yield channels than AsLOV2, presumably because of the differing structure and dynamics of the surrounding LOV protein scaffolding (Figure 1). A comparable D_{447}* lifetime (2.2 ns) was estimated by Losi et al. from fluorescence lifetime imaging microscopy (FLIM) under two-photon excitation of YtvA in live *E. coli* cells.[43]

Three phases in the secondary signals are observed (Figure 5) and are ascribed to the evolution of three coexisting triplet populations: ^{I}T*, ^{II}T*, and ^{III}T*. A fast-decaying 200 ns ^{I}T* population (with a 38% amplitude) is nonproductive and decays exclusively into the original D_{447} population with no measurable S_{390} population generated as confirmed by the identical EADS for this phase and the triplet spectrum from the ultrafast data prior to the generation of any S_{390} (Figure S3C of the Supporting Information). A second ^{II}T* population (with a 57% occupation) is ascribed to the slower 1.6 μs decay phase and exclusively generates all of the observed S_{390} population. A third weak (5%) and presumed nonproductive population (i.e., decays only into D_{447} but cannot be resolved in these data) resembles a persistent triplet state (Figure 5, >10 μs) with no resolvable decay and is ascribed to a long-lived ^{III}T* triplet (~300 μs) population similar to those observed in cysteine-less mutants of CrLOV2 domains (Table S1 of the Supporting Information).[57] The origin of this weak population in YtvA is unknown. No nonlinear excitation power features of the signals were observed (Figure S5 of the Supporting Information), which excludes this population resulting from a contaminating multiphoton ionization pathway.[58]

The inhomogeneous nature of the secondary dynamics (with three coexisting T* populations) provides an upper bound of 57% for the quantum yield (Φ_{adduct}) for generating the S_{390} adduct from the triplet populations assuming the ^{II}T* population has a 100% yield (Figure 7C, dashed red curve). Previously, Losi et al. estimated the Φ_{adduct} at 30%, which requires the ^{II}T* population to have a a Φ_{adduct} of ≈50% (assuming a near-unity ISC quantum yield).[5] Despite this, the estimate of Φ_{adduct} of 100% used in target analysis of the data presented here was selected to ensure comparable amplitudes of the D_{447} bleaches in both the T* and S_{390} SADS (Figure 7B, inset). The bleach contribution to the SADS of both populations strongly resembles the features of the D_{447} absorption (dashed curve), which suggests that no absorption (from either T* or S_{390}) overlaps the bleach (or is completely flat across the bleach).[59] This, in turn, indicates that the bleach amplitude is a valid metric for quantifying the relative amplitude of non-ground-state YtvA population (i.e., that is the instantaneous relative amplitude of T* and S_{390} populations) after excitation. Consequently, a Φ_{adduct} in the global analysis decreasing by half, to agree with the estimate of Losi et al., would double the relative amplitude of the estimated SADS for the S_{390} spectrum. This SADS would exhibit a 2-fold higher amplitude of the bleach of the S_{390} than the bleach of the T* SADS (because the terminal adduct spectrum scales linearly with both Φ_{adduct} and adduct extinction, also known as Beer's law).[47] It is unlikely that the bleaches of both samples would differ 2-fold for the T* and S_{390} populations and are likely comparable in amplitude, so we prefer to use the Φ_{adduct} of 100% for the ^{II}T* population, which gives a total Φ_{adduct} of 57% considering all three triplet populations.

The underlying molecular-level properties that distinguish the three T* populations are unresolved. Because the dynamic equilibration of the Cys occurs on the subnanosecond time scale, this inhomogeneity mechanism, which modulates ISC kinetics in the primary dynamics signals, will "average out" on the slower microsecond time scale;[28] hence, the influence of other local interactions with the FMN cofactor, such as hydrogen bonding and van der Waals interactions, on cysteinyl–FMN adduct formation kinetics must be considered. This may include altered conformational distributions of the flavin and the cysteine and a slow, large scale, structural change that facilitates the faster ISC dynamics in the ^{I}T* population to re-form D_{447}, because this triplet population is demonstratively unproductive.

Light-Adapted S_{390} Photodynamics. In contrast to the complex models used to analyze the signals from the dark-adapted state of YtvA, the primary signals generated after excitation of the S_{390} adduct state were analyzed only within a simpler four-state sequential model (e.g., EADS1 → EADS2, EADS2 → EADS3, and EADS3 → EADS4) (Figure 8A). Both the raw data (Figure S6 of the Supporting Information) and the estimated EADS from their analysis (Figure 8B) qualitatively resemble the signals measured for AcLOV2 by Kennis and co-workers,[26] who also analyzed their data with a four-state

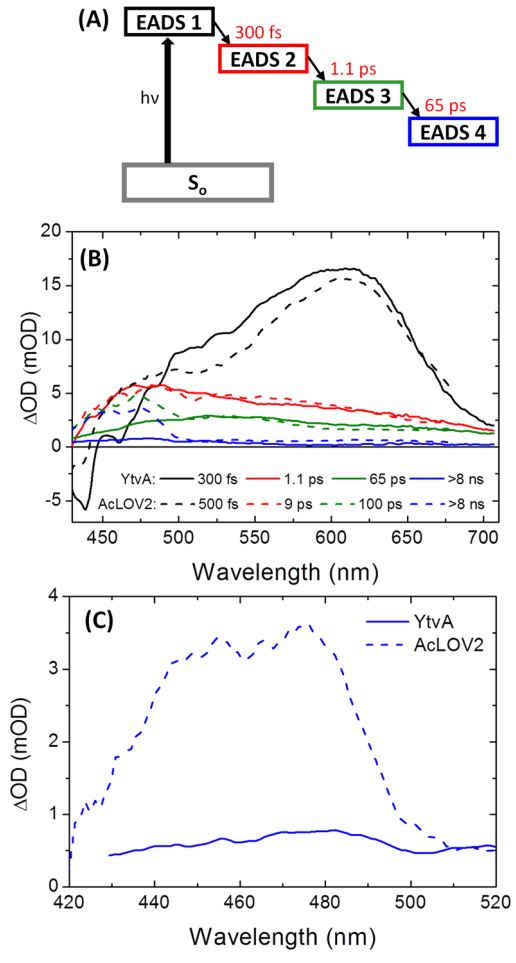

Figure 8. Sequential four-compartment EADS analysis of the primary (<8 ns) transient signals of the S_{390} state in full-length YtvA with 400 nm excitation. (A) Sequential model with parameters for YtvA indicated. (B) Dashed curve lines are the EADS from AcLOV2 of Kennis et al. (also with 400 nm excitation).[26] All EADS are scaled by the same factor (i.e., all steps are equally accelerated in YtvA and AcLOV2). (C) Long-lived (>100 μs) EADS4 for YtvA-LOV (solid blue curve) and AcLOV (dashed blue curve) are contrasted to emphasize the reduced adduct dissociation yield in YtvA.

dx.doi.org/10.1021/bi4012258 | *Biochemistry* 2013, 52, 7951–7963

Table 2. Global Analysis Parameters of the Transient Signals of Full-Length YtvA and AsLOV2

	D_{447} Excitation Dynamics					
	target analysis					
	primary dynamics			secondary dynamics		
	τ_{vib}[a] for D_{447}** → D_{447}*	τ_{ISC} for D_{447}* → T*	Φ_{ISC}[b]	τ_I for ^{I}T* → D_{447}	τ_{II} for ^{II}T* → S_{390}	Φ_{adduct}[c]
YtvA						
D_{447}*	1 ps	2.14 ns	78%			
^{I}T* (38%)	–	–	–	200 ns	*e*	0
^{II}T* (57%)	–	–	–	*e*	1.6 μs	100%
^{III}T* (5%)	–	–	–	>100 μs[f]	*e*	–
	S_{390} Excitation Dynamics					
	sequential analysis					
	τ_1 (fs)	τ_2 (ps)	τ_3 (ps)	τ_4	Φ_{dis}[d] (%)	
YtvA	300	1.1	64	∞	<2.5	
AcLOV2	500	9	100	∞	25[e]	

[a]Vibrational relaxation is observed only in the 400 nm-initiated signals. [b]Φ_{ISC} is estimated via comparison to AsLOV2 as the reference sample with a value of 65%.[27] [c]Φ_{adduct} is estimated under the assumption that the bleach of the S_{390} spectrum is comparable in amplitude to the bleach in the T* spectrum, which requires a 100% quantum yield for the productive triplet population (Figure 7B, inset). [d]The dissociation yield is estimated via comparison of terminal spectra of AcLOV2 with a Φ_{dis} of 25% and YtvA.[26] [e]No resolvable pathway is observed. [f]No measurable decay of this population was resolved up to the 100 μs experimental temporal window.

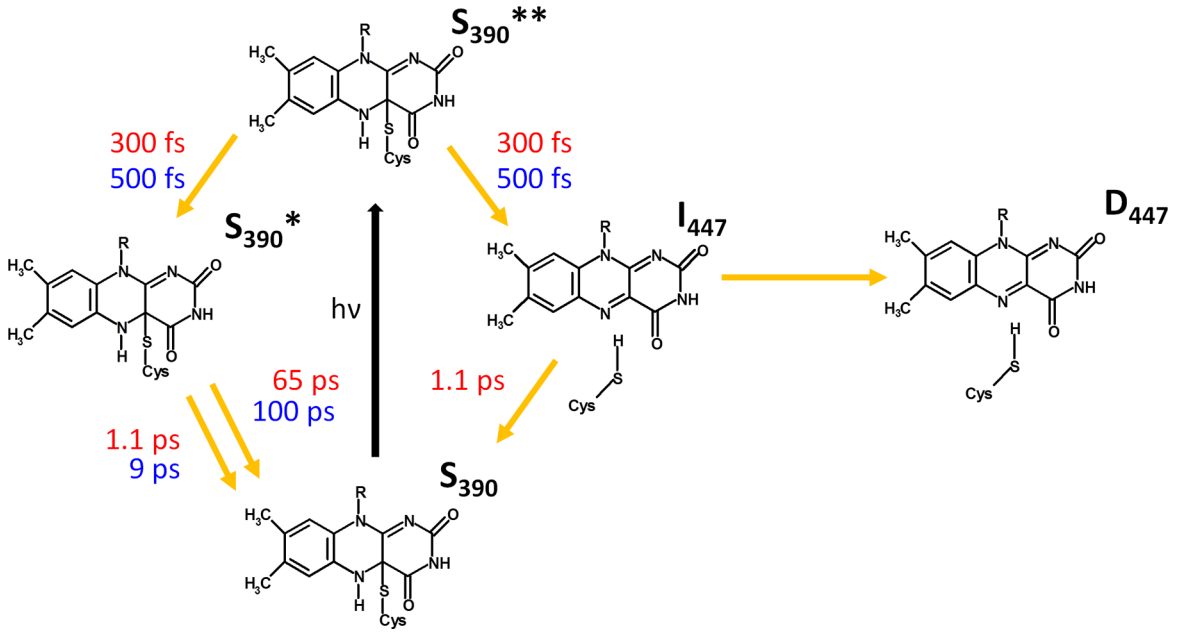

Figure 9. Proposed model for the interpretation of the sequential EADS analysis of the ultrafast light-adapted photodynamics of full-length YtvA and AcLOV2. The apparent time constants are colored red for YtvA and blue for AcLOV2; they do not represent the microscopic time constants estimated from a target analysis (e.g., Figure 7A). The evolution of I_{447} into D_{447} takes <10 ns and presumably requires large scale protein rearrangements to occur. An additional state is involved between I_{447} and D_{447} to account for the finite branching yield, while addressing the slower kinetics necessary in re-forming D_{447}. Because we have not directly resolved this hidden state, this state is not shown here.

sequential model. Two features are of immediate interest upon comparison of the analysis of the two samples: (1) the terminal (i.e., on a 10 ns time scale) photodissociation yield and (2) the respective time scales, with 2-fold faster dynamics for YtvA than for AcLOV2 (Table 2).

While the spectra (EADS1) of the first photoexcited populations for both YtvA and AcLOV2 are nearly identical (Figure 8B, black curves), the terminal spectra (EADS) differ greatly (Figure 8C, blue curves). The final spectrum for AcLOV2 (dashed blue curve) exhibits characteristic features of the D_{447} dark-adapted FMN population (or specifically the I_{447} − S_{390} difference spectrum) between 420 and 500 nm (Figure 2B). In stark contrast, the final spectrum for YtvA (solid blue curve) has a distinctly lower amplitude of this photogenerated I_{447} population (Figure 8C), indicating a significantly lower photodissociation yield (Φ_{dis}) for YtvA, compared to that of AcLOV2. Assuming comparable extinction coefficients for the respective I_{447} and S_{390}* populations for both LOV domains, and considering an average Φ_{dis} of 25 ± 5% estimated by Kennis et al.,[26] YtvA has approximately 10% of AcLOV2's yield or a 2.5% absolute Φ_{dis} for generating I_{447}. This value is close to the 2% estimate of Hellingwerf and co-workers[44] and the 4.9% estimate of Losi et al.[43] Hence, the observed decreased efficiency of the light-activated recovery dynamics of YtvA

dx.doi.org/10.1021/bi4012258 | *Biochemistry* 2013, 52, 7951−7963

originates from the primary dissociation dynamics and not from subsequent evolution like the inhomogeneous secondary dynamics of the respective dark-adapted signals (Figure 7).

Interpreting how the evolution of the S_{390}-derived ultrafast signals results in a decreased dissociation yield for generating the I_{447} population is difficult because the nature of the excited-state spectra is unknown (in contrast to the dynamics upon excitation of the dark-adapted state). To continue this comparison of the different LOV domains' light-adapted signals, a "working model" is constructed to interpret the EADS analysis (Figure 9), which was formulated by considering only the AcLOV2 signals (Figure 8B, dashed curves) and their comparison to the YtvA data; this is not a target analysis estimated by modeling YtvA signals directly. In this model, the initial spectrum in the sequential analysis (EADS1) is ascribed to an excited-state S_{390}** population, photogenerated prior to adduct dissociation, and is most likely vibrationally excited or structurally distorted, e.g., close to the Franck−Condon geometry (Figure 8B, black dashed curve). The sequential analysis tracks the decay of S_{390}** (∼500 fs) to the formation of EADS2 (red dashed curve) that peaks at 475 nm with a long positive absorption extending to the low-energy limit of the spectral window. The subsequent EADS2 to EADS3 evolution (red dashed vs green dashed curves) is more comparable to the EADS1 to EADS2 evolution with largely a loss of signal amplitude. However, a smaller loss of absorption is observed from 425 to 500 nm where the nascent I_{447} absorbs with a relatively greater loss of the positive ESA at >500 nm. This suggests that EADS2 consists of two coexisting populations generated from S_{390}** (Figure 8C): an I_{477} population (from 425 to 500 nm) and a new excited-state S_{390}* population (from 425 to 700 nm, but mostly >500 nm) with an ESA that is blue-shifted from the S_{390}** population. The S_{390}* population may be a vibrationally or structurally relaxed excited-state population or perhaps even a secondary ground-state population (e.g., FMN radicals from hemolytic breakage of the FMN−cysteinyl bond or protonated FMN due to the failed transfer of a proton from C4a to the cysteine after heterolytic adduct breakage).

The weak decrease in the absorption in the I_{447} spectral region after the decay of S_{390}** suggests that most (or all) of the dissociated I_{447} photoproduct is generated on the subpicosecond time scale (i.e., from the decay of S_{390}**), and the subsequent decays are largely ascribed to the decay kinetics of the coexisting nondissociated S_{390}* population(s). Comparison of EADS3 and EASD4 (blue vs green dashed curves) further supports this hypothesis with primarily loss of the red ESA with a weak loss of absorption in the I_{447} region (ascribed to weak overlapping absorption of S_{390}*) and the persistence of I_{447} on the ultrafast time scale. Unfortunately, the data were not of sufficient quality to use this scheme as a target model within a global analysis like what was done with the signals from the dark-adapted state after light activation (described above). Despite this, the model captures the essence of the sequential analysis within a simplified description.

Extending the working model in Figure 9 to the YtvA EADS analysis results in a different outcome than in AcLOV2. Because the S_{390}** population in YtvA is spectrally similar to the S_{390}** population in AcLOV2 (Figure 8B, black curves) as is EADS2 (red curve), the dissociation reaction occurs with comparable yields (i.e., similar amplitudes of the I_{447} and S_{390}* populations in EADS2), albeit considerably faster in YtvA (300 fs vs 500 fs in AcLOV2). However, the EADS2 to EADS3 (green curves) evolution is markedly different for YtvA and AcLOV2, with the EADS3 of YtvA missing most of the I_{447} absorption (425−500 nm) that existed in EADS2. This loss of the I_{447} population in EADS3 extends to EADS4 (Figure 8C), indicating no new (or little) I_{447} is generated on slower time scales. Interestingly, the ESA of the coexisting S_{390}* population (>500 nm) is comparable for the two LOV domains.

The decay of the nascent I_{447} population on the 1.1 ps time scale in YtvA indicates that the FMN and the freed cysteine recombine after dissociation. This is a common observation in condensed phase photodissociation studies due to "caging" of the species by the local environment that preserved the orientation and proximity of dissociated products to facilitate recombination. It is clear from the signals that this recombination pathway proceeds through a mechanism different from the mechanism involved when the dark-adapted state is activated with light (i.e., $D_{447} \rightarrow D_{447}^* \rightarrow T^* \rightarrow S_{390}$) because no clear signatures of D_{447}* or T* were observed in the signals (Figure 7B).

For AcLOV2, the recombination process is hindered in some manner, resulting in a higher dissociation quantum yield and, thus, photoswitching activity. One explanation for this is that the protein environment surrounding the FMN may exert stronger "stresses" on the adduct (and its dissociated species) in type I LOV domains like AcLOV2 than in type II domains like YtvA. Hence, once the cysteinyl−FMN bond is cleaved (after the decay of S_{390}**), the cysteine is removed or reoriented away from the local volume region surrounding C4a of the FMN. This hinders recombination of the nascent photoproducts and results in higher photoswitching activity. In contrast, the cysteine in YtvA may be held closer to the FMN after photodissociation and facilitate the regeneration of the S_{390} adduct. The mechanism of this adduct formation reaction is unclear, but because proton transfer is a necessary step in adduct formation, a hypothesis is that the YtvA system may still be primed for adduct formation after dissociation by hindering extraction of hydrogen from the FMN in a manner similar to the imidazole-mediated recovery mechanism.

The different adduct disruption yields for the AcLOV2 and YtvA photodynamics may be ascribed to the different structures (Figure 1) of the two domains or to the associated protein dynamics of those proteins, including the translational and rotational motions of the cysteine. These motions were already demonstrated to strongly affect the ISC kinetics in AsLOV2.[28] Molecular dynamics simulations of AsLOV2 predict an ∼1 ns isomerization time scale for C62 in the dark-adapted state of the protein,[28] which is considerably slower than the time scale of 1 ps observed here. This may also be facilitated by the hydrogen bonding of the nearby residues (Q123, N104, and N92) that may be stronger in the adduct state of YtvA than in that of AcLOV2, because of a shift in the position of the FMN after photodissociation. Clearly, the photodynamics between YtvA and the type I LOV domains differ (including lifetimes and yields), which are likely the result of differing local photodynamics originating from the differing structures and protein fluctuation of the two types of domains.

■ CONCLUSION

The structure and thermal recovery kinetics of the LOV domain in full-length YtvA are significantly different from those in type I LOV domain systems, which extends to key differences in the primary (100 fs to 10 ns) and secondary (10 ns to 100 μs) photodynamics, as demonstrated here with time-resolved absorption spectroscopy. Figure 10 integrates the

dx.doi.org/10.1021/bi4012258 | Biochemistry 2013, 52, 7951−7963

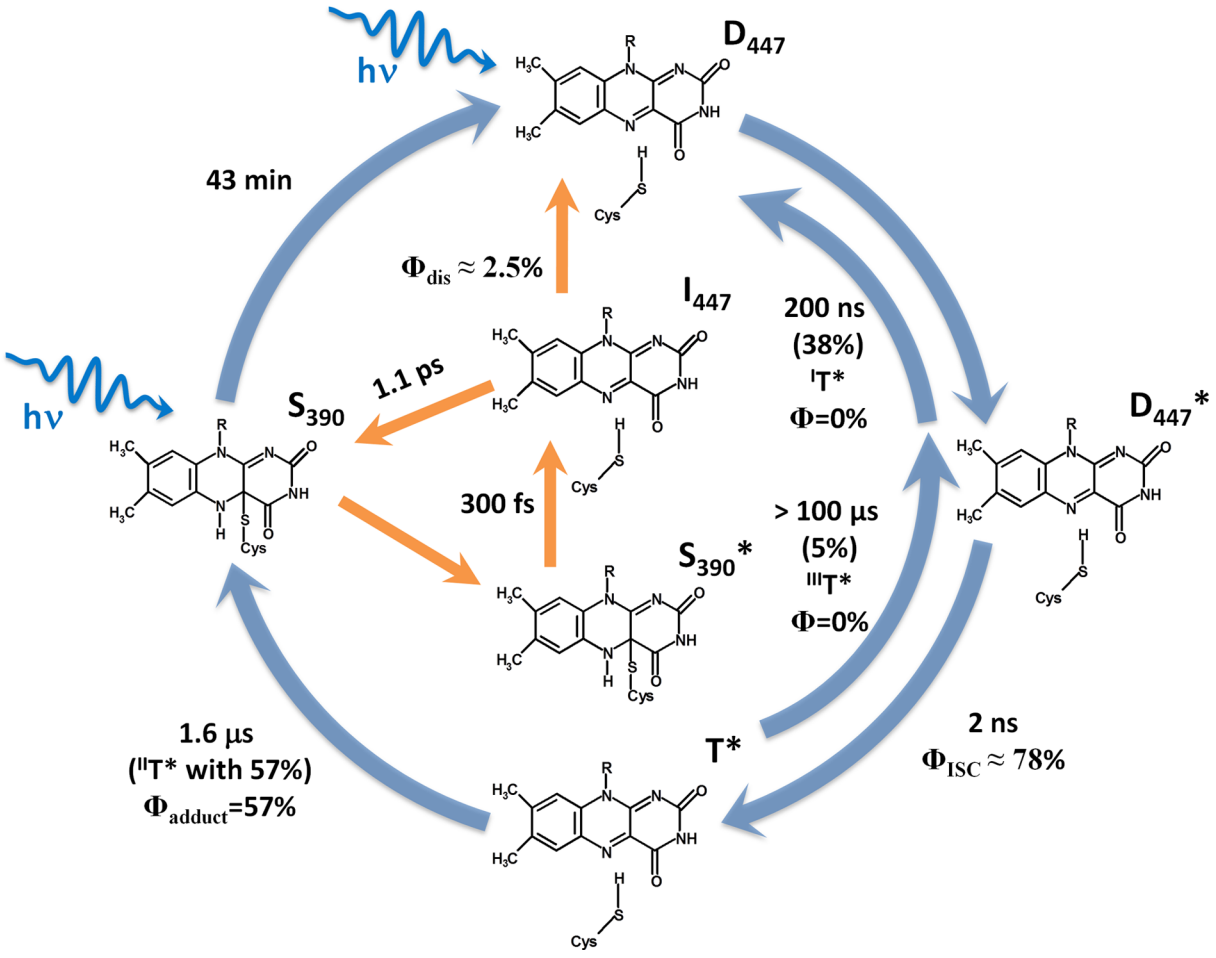

Figure 10. Simplified YtvA photocycle after blue light excitation of the dark-adapted D_{447} population (blue arrows) and after blue light excitation of the light-adapted S_{390} adduct population (orange arrows). Kinetic parameters are listed in Table 2. The arrows signify either single or multiple populations co-evolving (see Figures 7–9 for a more accurate representation of the underlying dynamics).

results of all three transient data sets within a simple scheme. Photoexcitation of the dark-adapted D_{447} state generates two singlet exited-state D_{447}* populations that decay with high yields (~100%) into three long-lived triplet populations. The fast-decaying (200 ns) ^{I}T* population exclusively re-forms the D_{447} state, while the second slower (1.6 μs) ^{II}T* population generates the S_{390} adduct state via the formation of a covalent bond between the sulfur atom of a nearby cysteine and C4a of the FMN molecule. The third ^{III}T* population is long-lived with no clear photoactivity on the time scale of the experiment. The S_{390} adduct state persists on a 43 min time scale at room temperature, before the eventual regeneration of the dark-adapted D_{447} population. In contrast to type I LOV domains, this recovery time scale is only weakly accelerated by the introduction of imidazole probably because of an obstructed cavity between Cα and Hβ that hinders access of imidazole to the FMN chromophore (Table 1). Photoexcitation of the S_{390} state of YtvA results in weak efficiency in regenerating the I_{477} population (orange arrows), in contrast to the type I AcLOV2 domain. This smaller photoactivity originates from the ultrafast recombination (~1.1 ps) of the nascent I_{447} population formed after photodissociation of the S_{390} adduct. The portion of I_{447} that does not recombine (~3%) evolves into D_{447} on a slower, unresolved time scale as estimated independently from the analysis of steady-state measurements.[44] This recombination mechanism that re-forms the S_{390} adduct state is much less efficient in type I LOV domains, which substantially increases the photoswitching efficiency in these latter systems.

■ ASSOCIATED CONTENT

Supporting Information

Seven figures. This material is available free of charge via the Internet at http://pubs.acs.org.

■ AUTHOR INFORMATION

Corresponding Author

*Department of Chemistry, University of California at Davis, Davis, CA 95616. E-mail: dlarsen@ucdavis.edu. Telephone: (530) 754-9075.

Author Contributions

S.-H.S. and D.M. contributed equally to this manuscript.

Funding

This work was supported by Career Development Award CDA0016/2007-C from the Human Frontiers Science Organization (to D.S.L.).

Notes

The authors declare no competing financial interest.

■ ACKNOWLEDGMENTS

Thanks to Chet Price and Margaret S. Brody (University of California at Davis) for the gift of YtvA-LOV for the dark

recovery studies. Also, we thank John Kennis (Vrije Universiteit, Amsterdam, The Netherlands) for generously providing the analysis and signals for the light-adapted AcLOV2 dynamics and for constructive discussions and Jos Arents for his help in protein purification and sample preparation.

■ ABBREVIATIONS

TA, transient absorption; LOV, light−oxygen−voltage; STAS, sulfate transporter and anti-σ factor antagonist; PAS, Per-Arnt-Sim (PAS, for period circadian protein, Ah receptor nuclear translocator protein, and Ssingle-minded protein); σ^B, sigma factor; AsLOV2, LOV domain from *Av. sativa*; AcLOV2, LOV domain from *A. capillus-veneris*; AcLOV2, LOV2 domain extracted from the phy3 receptor of *A. capillus-veneris*; CrLOV1, LOV domain from *C. reinhardtii*; Φ_{ISC}, intersystem crossing (or triplet) yield; Φ_{adduct}, adduct quantum yield; Φ_{dis}, photodissociation quantum yield; S_{390}, light-adapted state of LOV domains; D_{447}, dark-adapted state of LOV domains; D447*, singlet excited state of the dark-adapted state; T*, triplet excited state; I_{447}, primary photodissociation photoproduct; S_{390}**, initial singlet excited state of S_{390}; S_{390}*, vibrationally or structurally relaxed singlet excited state of S_{390}; FMN, flavin mononucleotide chromophore; Nd:YAG, neodymium-doped yttrium aluminum garnet; SADS, species-associated difference spectra; EADS, evolution-associated difference spectra; PDB, Protein Data Bank.

■ REFERENCES

(1) Moeglich, A., and Moffat, K. (2010) Engineered photoreceptors as novel optogenetic tools. *Photochem. Photobiol. Sci. 9*, 1286.

(2) Christie, J., Gawthorne, J., Young, G., Fraser, N., and Roe, A. (2012) LOV to BLUF: Flavoprotein contributions to the optogenetic toolkit. *Mol. Plant 5*, 533−544.

(3) Briggs, W. R., and Spudich, J. L. (2005) *Handbook of Photosensory Receptors*, Wiley-VCH Verlag GmbH & Co. KGaA, Berlin.

(4) van der Horst, M., and Hellingwerf, K. J. (2004) Photoreceptor proteins, "star actors of modern times": A review of the functional dynamics in the structure of representative members of six different photoreceptor families. *Acc. Chem. Res. 37*, 13−20.

(5) Losi, A., Polverini, E., Quest, B., and Gartner, W. (2002) First Evidence for Phototropin-Related Blue-Light Receptors in Prokaryotes. *Biophys. J. 82*, 2627−2634.

(6) Hecker, M., Pané-Farré, J., and Uwe Völker, U. (2007) SigB-Dependent General Stress Response in *Bacillus subtilis* and Related Gram-Positive Bacteria. *Annu. Rev. Microbiol. 61*, 215−236.

(7) Price, C., Fawcett, P., Cérémonie, H., Su, N., Murphy, C., and Youngman, P. (2001) Genome-wide analysis of the general stress response in *Bacillus subtilis*. *Mol. Microbiol. 41*, 757−774.

(8) Nannapaneni, P., Hertwig, F., Depke, M., Hecker, M., Mäder, U., Völker, U., Leif Steil, L., and van Hijum, S. A. F. T. (2012) Defining the structure of the general stress regulon of *Bacillus subtilis* using targeted microarray analysis and random forest classification. *Microbiology 158*, 696−707.

(9) Petersohn, A., Brigulla, M., Haas, S., Hoheisel, J. D., Völker, U., and Hecker, M. (2001) Global Analysis of the General Stress Response of *Bacillus subtilis*. *Microbiology 183*, 5617−5631.

(10) Cao, M., and Helmann, J. D. (2002) Regulation of the *Bacillus subtilis* bcrC Bacitracin Resistance Gene by Two Extracytoplasmic Function σ Factors. *J. Bacteriol. 184*, 6123.

(11) Avila-Pérez, M., Hellingwerf, K. J., and Kort, R. (2009) Blue light activates the σB-dependent stress response of *Bacillus subtilis* via YtvA. *J. Bacteriol. 188*, 6411−6414.

(12) Gaidenko, T., Kim, T. J., Weigel, A., Brody, M., and Price, C. (2006) The Blue-Light Receptor YtvA Acts in the Environmental Stress Signaling Pathway of *Bacillus subtilis*. *J. Bacteriol. 188*, 6387−6395.

(13) Chen, C. C., Lewis, R. J., Harris, R., Yudkin, M. D., and Delumeau, O. (2003) A supramolecular complex in the environmental stress signalling pathway of *Bacillus subtilis*. *Mol. Microbiol. 49*, 1657−1669.

(14) Marles-Wright, J., Grant, T., Delumeau, O., van Duinen, G., Firbank, S., Lewis, P., Murray, J., Newman, J., Quin, M., Race, P., Rohou, A., Tichelaar, W., van Heel, M., and Lewis, R. (2008) Molecular architecture of the "stressosome," a signal integration and transduction hub. *Science 322*, 5898.

(15) Akbar, S., Gaidenko, T. A., Kang, C. M., O'Reilly, M., Devine, K. M., and Price, C. W. (2001) New family of regulators in the environmental signaling pathway which activates the general stress transcription factor σ(B) of *Bacillus subtilis*. *J. Bacteriol. 183*, 1329−1338.

(16) Jurk, M., Schramm, P., and Schmieder, P. (2013) The blue-light receptor YtvA from *Bacillus subtilis* is permanently incorporated into the stressosome independent of the illumination state. *Biochem. Biophys. Res. Commun. 432*, 499−503.

(17) Van der Steen, J. B., Ávila-Pérez, M., Knippert, D., Vreugdenhil, A., van Alphen, P., and Hellingwerf, K. (2013) Differentiation of Function among the RsbR Paralogs in the General Stress Response of *Bacillus subtilis* with Regard to Light Perception. *J. Bacteriol. 194*, 1708−1716.

(18) Aravind, L., and Koonin, E. V. (2000) The STAS domain: A link between anion transporters and antisigma-factor antagonists. *Curr. Biol. 10*, R53−R55.

(19) Pellequer, J. L., Wager-Smith, K. A., Kay, S. A., and Getzoff, E. D. (1998) Photoactive yellow protein: A structural prototype for the three-dimensional fold of the PAS domain superfamily. *Proc. Natl. Acad. Sci. U.S.A. 95*, 5884−5890.

(20) Zhulin, I., Taylor, B., and Dixon, R. (1997) PAS domain S-boxes in Archaea, Bacteria and sensors for oxygen and redox. *Trends Biochem. Sci. 22*, 331−333.

(21) Cabral, J. H. M., Lee, A., Cohen, S. L., Chait, B. T., Li, M., and Mackinnon, R. (1998) Crystal structure and functional analysis of the HERG potassium channel N terminus: A eukaryotic PAS domain. *Cell 95*, 649−655.

(22) Gong, W. M., Hao, B., Mansy, S. S., Gonzalez, G., Gilles-Gonzalez, M. A., and Chan, M. K. (1998) Structure of a biological oxygen sensor: A new mechanism for heme-driven signal transduction. *Proc. Natl. Acad. Sci. U.S.A. 95*, 15177−15182.

(23) Crosson, S., and Moffat, K. (2001) Structure of a flavin-binding plant photoreceptor domain: Insights into light-mediated signal transduction. *Proc. Natl. Acad. Sci. U.S.A. 98*, 2995−3000.

(24) Christie, J. M., Salomon, M., Nozue, K., Wada, M., and Briggs, W. R. (1999) LOV (light, oxygen, or voltage) domains of the blue-light photoreceptor phototropin (nph1): Binding sites for the chromophore flavin mononucleotide. *Proc. Natl. Acad. Sci. U.S.A. 96*, 8779−8783.

(25) Kawai, H., Kanegae, T., Christensen, S., Kiyosue, T., Sato, Y., Imaizumi, T., Kadota, A., and Wada, M. (2002) Responses of ferns to red light are mediated by an unconventional photoreceptor. *Nature 421*, 287−290.

(26) Kennis, J. T., van Stokkum, I. H., Crosson, S., Gauden, M., Moffat, K., and van Grondelle, R. (2004) The LOV2 domain of phototropin: A reversible photochromic switch. *J. Am. Chem. Soc. 126*, 4512−4513.

(27) Kennis, J. T., Crosson, S., Gauden, M., van Stokkum, I. H., Moffat, K., and van Grondelle, R. (2003) Primary reactions of the LOV2 domain of phototropin, a plant blue-light photoreceptor. *Biochemistry 42*, 3385−3392.

(28) Song, S.-H., Freddolino, P., Nash, A. M., Carroll, E. C., Schulten, K., Gardner, K. H., and Larsen, D. S. (2011) Modulating LOV Domain Photodynamics with a Residue Alteration outside the Chromophore Binding Site. *Biochemistry 50*, 2411−2423.

(29) Swartz, T. E., Corchnoy, S. B., Christie, J. M., Lewis, J. W., Szundi, I., Briggs, W. R., and Bogomolni, R. A. (2001) The photocycle of a flavin-binding domain of the blue light photoreceptor phototropin. *J. Biol. Chem. 276*, 36493−36500.

(30) Crosson, S., and Moffat, K. (2002) Photoexcited structure of a plant photoreceptor domain reveals a light-driven molecular switch. *Plant Cell 14*, 1067−1075.
(31) Losi, A., Quest, B., and Gartner, W. (2003) Listening to the blue: The time-resolved thermodynamics of the bacterial blue-light receptor YtvA and its isolated LOV domain. *Photochem. Photobiol. Sci. 2*, 759−766.
(32) Zoltowski, B. D., Vaccaro, B., and Crane, B. R. (2009) Mechanism-based tuning of a LOV domain photoreceptor. *Nat. Chem. Biol. 5*, 827−834.
(33) Moeglich, A., and Moffat, K. (2007) Structural basis for light-dependent signaling in the dimeric LOV domain of the photosensor YtvA. *J. Mol. Biol. 373*, 112−126.
(34) Crosson, S., Rajagopal, S., and Moffat, K. (2003) The LOV domain family: Photoresponsive signaling modules coupled to diverse output domains. *Biochemistry 42*, 2−10.
(35) Buttani, V., Losi, A., Eggert, T., Krauss, U., Jaeger, K. E., Cao, Z., and Gartner, W. (2007) Conformational analysis of the blue-light sensing protein YtvA reveals a competitive interface for LOV-LOV dimerization and interdomain interactions. *Photochem. Photobiol. Sci. 6*, 41−49.
(36) Suzuki, N., Naoki Takaya, N., Hoshino, T., and Nakamura, A. (2007) Enhancement of a σB-dependent stress response in *Bacillus subtilis* by light via YtvA photoreceptor. *J. Gen. Appl. Microbiol. 53*, 81−88.
(37) Jurk, M., Dorn, M., and Schmieder, P. (2011) Blue Flickers of Hope: Secondary Structure, Dynamics and Putative Dimerisation Interface of the Blue-Light Receptor YtvA from *Bacillus subtilis*. *Biochemistry 50*, 8163−8171.
(38) Harper, S. M., Neil, L. C., and Gardner, K. H. (2003) Structural basis of a phototropin light switch. *Science 301*, 1541−1544.
(39) Harper, S. M., Christie, J. M., and Gardner, K. H. (2004) Disruption of the LOV-Jα helix interaction activates phototropin kinase activity. *Biochemistry 43*, 16184−16192.
(40) Berberan-Santos, M. N. (2000) External heavy-atom effect on fluorescence kinetics. *PhysChemComm 3*, 18−23.
(41) Chandra, A. K., Turro, N. J., Lyons, A. L., and Stone, P. (1978) Intra-Molecular External Heavy-Atom Effect In Bromonorbornenes, Benzonorbornenes and Naphthonorbornenes. *J. Am. Chem. Soc. 100*, 4964−4968.
(42) Alexandre, M. T. A., van Grondelle, R., Hellingwerf, K. J., Robert, B., and Kennis, J. T. M. (2008) Perturbation of the ground-state electronic structure of FMN by the conserved cysteine in phototropin LOV2 domains. *Phys. Chem. Chem. Phys. 10*, 6693−6702.
(43) Losi, A., Gartner, W., Raffelberg, S., Zanacchi, F. C., Bianchini, P., Diaspro, A., Mandalari, C., Abbruzzetti, S., and Viappiani., C. (2013) A photochromic bacterial photoreceptor with potential for super-resolution microscopy. *Photochem. Photobiol. Sci. 12*, 231−235.
(44) van der Steen, J. B., Nakasone, Y., Hendriks, J., and Hellingwerf, K. J. (2013) Modeling the functioning of YtvA in the general stress response in Bacillus subtilis. *Mol. BioSyst. 9*, 2331−2343.
(45) Carroll, E. C., Compton, O. C., Madsen, D., Osterloh, F. E., and Larsen, D. S. (2008) Ultrafast carrier dynamics in exfoliated and functionalized calcium niobate nanosheets in water and methanol. *J. Phys. Chem. C 112*, 2394−2403.
(46) Holzwarth, A. R. (1996) Data Analysis of Time-Resolved Measurements. In *Biophysical techniques in photosynthesis* (Amesz, J., and Hoff, A. J., Eds.) pp 75−92, Springer, Dordrecht, The Netherlands.
(47) van Stokkum, I. H. M., Larsen, D. S., and van Grondelle, R. (2004) Global and target analysis of time-resolved spectra. *Biochim. Biophys. Acta 1657*, 82−104.
(48) Kim, P. W., Freer, L. H., Rockwell, N. C., Martin, S. S., Lagarias, J. C., and Larsen, D. S. (2012) Femtosecond Photodynamics of the Red/Green Cyanobacteriochrome NpR6012g4 from *Nostoc punctiforme*. 1. Forward Dynamics. *Biochemistry 51*, 608−618.
(49) Kim, P. W., Freer, L. H., Rockwell, N. C., Martin, S. S., Lagarias, J. C., and Larsen, D. S. (2012) Femtosecond Photodynamics of the Red/Green Cyanobacteriochrome NpR6012g4 from *Nostoc punctiforme*. 2. Reverse Dynamics. *Biochemistry 51*, 619−630.
(50) Mueller, F. (1991) *Chemistry and biochemistry of flavoenzymes*, CRC Press, Boca Raton, FL.
(51) Alexandre, M. T., Arents, J. C., van Grondelle, R., Hellingwerf, K. J., and Kennis, J. T. (2007) A base-catalyzed mechanism for dark state recovery in the *Avena sativa* phototropin-1 LOV2 domain. *Biochemistry 46*, 3129−3137.
(52) Christie, J. M., Corchnoy, S. B., Swartz, T. E., Hokenson, M., Han, I. S., Briggs, W. R., and Bogomolni, R. A. (2007) Steric interactions stabilize the signaling state of the LOV2 domain of phototropin 1. *Biochemistry 46*, 9310−9319.
(53) Gauden, M., van Stokkum, I. H. M., Key, J. M., Luhrs, D. C., Van Grondelle, R., Hegemann, P., and Kennis, J. T. M. (2006) Hydrogen-bond switching through a radical pair mechanism in a flavin-binding photoreceptor. *Proc. Natl. Acad. Sci. U.S.A. 103*, 10895−10900.
(54) Wolf, M. M. N., Schumann, C., Gross, R., Domratcheva, T., and Diller, R. (2008) Ultrafast Infrared Spectroscopy of Riboflavin: Dynamics, Electronic Structure, and Vibrational Mode Analysis. *J. Phys. Chem. B 112*, 13424−13432.
(55) Stanley, R. J., and MacFarlane, A. W. (2000) Ultrafast excited state dynamics of oxidized flavins: Direct observations of quenching by purines. *J. Phys. Chem. A 104*, 6899−6906.
(56) Heelis, P. F., Parsons, B. J., Phillips, G. O., and Mckellar, J. F. (1981) The Flavin Sensitized Photo-Oxidation of Ascorbic-Acid: A Continuous and Flash-Photolysis Study. *Photochem. Photobiol. 33*, 7−13.
(57) Holzer, W., Penzkofer, A., Fuhrmann, M., and Hegemann, P. (2002) Spectroscopic characterization of flavin mononucleotide bound to the LOV1 domain of Phot1 from *Chlamydomonas reinhardtii*. *Photochem. Photobiol. 75*, 479−487.
(58) Larsen, D. S., Vengris, M., van Stokkum, I. H. M., van der Horst, M. A., de Weerd, F. L., Hellingwerf, K. J., and van Grondelle, R. (2004) Photoisomerization and photoionization of the photoactive yellow protein chromophore in solution. *Biophys. J. 86*, 2538−2550.
(59) Swartz, T., Corchnoy, S., Christie, J., Lewis, J., Szundi, I., Briggs, W., and Bogomolni, R. (2001) The Photocycle of a Flavin-binding Domain of the Blue Light Photoreceptor Phototropin. *J. Biol. Chem. 276*, 36493−36500.